Optimize the Properties of Carbon Nanotubes Synthesized using a Microwave Oven

AHMAD M. AL-DIABAT[1*], NATHEER A. ALGADRI[2], NASER M. AHMAD[3],
ADNAN H. ALRAJHI[3], ABDULSALAM ABUELSAMEN[4],
AMAL MOHAMED AHMED ALI[3], SALMA ABDULRHMAN AL-WASLI[3]
[1]Department of Physics,
Al-Zaytoonah University of Jordan,
Amman,
JORDAN

[2]Department of Physics,
Isra University,
Amman,
JORDAN

[3]School of Physics,
Universiti Sains Malaysia,
Penang,
MALAYSIA

[4]Aqaba University of Technology,
Aqaba,
JORDAN

**Corresponding Author*

Abstract: - In this paper, carbon nanotubes (CNT) are synthesized using the microwave oven method, which offers several advantages, including a simple, quick, inexpensive, and solvent-free growing method. To produce CNT, a mixture of graphite and ferrocene catalysts had to be flattened inside a microwave oven for five seconds at room temperature. CNT was produced using various ratios of graphite and ferrocene, and analyses indicated that a 70:30 graphite/ferrocene ratio produced better nanocrystalline CNT. To optimize CNT properties, five processes of purification were used to dispose of impurities like metal particles and support material from the as-produced carbon nanotubes. Raman spectroscopy, field emission scanning electron microscopy (FESEM), energy dispersive X-ray spectroscopy (EDX), X-ray diffraction (XRD), and Fourier transform infrared spectroscopy (FTIR) was used to characterize the CNTs both after and before purification.
After acid treatment and centrifugation, the amount of amorphous carbon and iron particles significantly decreased. Additionally, following the purification process, the I_D/I_G decreased by 0.14 and the I_{2D}/I_D increased by 0.55 for the purified CNTs. Furthermore, the FTIR spectra of the untreated and functionalized CNTs confirm the presence of carboxyl groups on pure CNTs and -OH moieties in sorbed water.

Key-Words: -CNT, functionalization, purification, nitric acid, microwave.

Received: February 8, 2023. Revised: May 23, 2023. Accepted: June 22, 2023. Published: July 19, 2023.

1 Introduction

Several methods for carbon nanotube (CNT) growth have been used to produce CNTs with the appropriate features. The techniques that are most frequently utilized are chemical vapor deposition (CVD), laser ablation, electrolysis, hydrothermal, and arc discharge, [1], [2].

Furthermore, the microwave oven technique is often employed since it is a simple and inexpensive method for the production of CNTs at ambient pressure and room temperature (RT). In contrast to the other techniques, the microwave oven technique is extremely quick and easy to implement, [3], [4].
All the synthesis methods produce CNTs that contain different impurities like carbon nanoparticles, amorphous carbon, metal particles, and other unwanted particles, [5], [6]. Subject to the type of impurity, a mixture of chemical and physical techniques is necessary to achieve complete purification. The main methods for the purification of CNTs include ultrasonication, oxidation, annealing, magnetic purification, acid treatment, centrifugation, filtration, and functionalization, [5], [7], [8], [9], [10]. Oxidation can be used to clean the metal surface and remove carbonaceous impurities (C-impurities), including amorphous carbon particles from carbon nanotubes. Wet and dry oxidation are two different types of oxidations. The wet oxidation treatment involves refluxing CNTs in strong acids such as H_2O_2, $HClO_4$, HNO_3, H_2SO_4+$KMnO_4$, and HNO_3+H_2SO_4. for 24 hours at RT. Dry oxidation is conducted under atmospheric air or oxygen gas at high temperatures (500–750 ^oC), [5], [11], [12].
In this study, carbon nanotubes were produced in one step using the conventional microwave oven for a short time in the absence of inert or feedstock gases. Then, a five-step purification process was used to improve the CNT's properties by eliminating impurities like metal particles and support material. The CNTs were characterized using different analytical techniques after and before purification.

2 Experimental Part

2.1 Synthesized CNT

The CNTs were synthesized using a method that makes use of a traditional microwave oven. To achieve the homogeneous distribution of microwave heat at every point inside the quartz boat, a mixture of graphite and ferrocene was put in quartz boats at various ratios (80:20, 70:30, 50:50, and 40:60), and when the pop light spark appeared, the microwave heating was turned off.

2.2 Carbon Nanotube Treatment

1 g of as-produced carbon nanotubes (R-CNT) were treated in 1 L of nitric acid (2.6 M HNO3) under stirring and blending at room temperature for 17 h (Fig. 1, step 1). The hydrophilicity of CNTs is enhanced as a result of the acid treatment, which enables chemical functional groups "(-OH)" to attach to the sidewalls of CNTs, [13].

Furthermore, it is employed in the purification process to remove metallic particles and unwanted material after exposing the metal surface to oxidation and sonication treatments. The acid dissolves the metal particle in the catalyst, while the nanotube remains suspended in the acid, [10], [14].
N nitric acid, CNTs, and other carbon particles are unaffected, whereas metal particles are removed. The benefits of using nitric acid include its low cost and effectiveness in removing metal particles. Contrarily, hydrochloric acid treatment slightly affects the structures and properties of CNTs, [5], [15], [16].

The ultrasonic process involved the use of ultrasound to suspend the highly agglomerated nanotubes. The ultrasonic process typically takes between 40 and 60 minutes (Fig. 1, step 2).
After the acid treatment, a supernatant of CNT was obtained by centrifuging at 10,000 rpm for 1 hour (Fig. 1, step 3), [8], and deionized water was used to rinse the solution many times until the pH reached 7. (Fig. 1, step 4). Finally, the as-produced CNTs were desiccated in a furnace at 70 ˚C for 72 h, as a result, functionalized and purified carbon nanotube (F-CNT) powder could be obtained (Fig. 1, step 5).

3 Result and Dissociation

3.1 As-produced CNT

3.1.1 Raman Spectroscopy Analysis

Fig. 2 illustrates the Raman spectrum of four CNT samples grown using different graphite/ferrocene ratios (80:20, 70:30, 50:50, and 40:60).

The well-ordered carbon atoms in the graphene layer are related to two separate bands at 1580 cm^{-1} (G-band), and all sp^2 carbon materials have defects (D) at 1330 cm^{-1}. Additionally, a 2D band of active CNTs was found to satisfy particular chirality requirements by double resonance. The intensity ratio for G to D bands (I_D/I_G), [17], which measures the degree of crystallinity and phase purity in the acquired samples, was used to describe the degree of ordered structure with respect to defects that were present in CNTs. A low I_D/I_G ratio suggested

that the graphitic structure of CNTs was well-ordered. Since the development of the 2D band in CNTs was very sensitive to an increase in defect density, the proposed CNTs' crystallinity and phase purity were determined using the value of I_{2D}/I_D, [18].

Table 1 provides the full-width half maximum (FWHM) of the G-band as well as the relative intensity ratios of the D-to-G and 2D-to-D bands derived from the Raman spectra shown in Fig. 2.

In comparison to the 80:20, 50:50, and 40:60 ratios, the CNTs made from a graphite/ferrocene combination with a 70:30 ratio had the highest values of I_{2D}/I_D and FWHM (G), as well as the lowest values of I_D/I_G.

The Raman spectra of the CNT powder are shown in Fig. 3 (a). It displayed two distinct, identical high-intensity peaks at 1333 and 1582 cm^{-1}. The G-asymmetries bands suggest that the spectrum has many peak components. Figure 3 (b) displays the de-convoluted Raman spectra of the carbon nanotube that were shown using the Lorentzian curve fit for the G band.

Asymmetric G and G+ components are visible in the Raman spectra of CNT samples with a 70:30 sample ratio at 1580 and 1615 cm^{-1}, respectively. The semiconducting component at 1580 cm^{-1} and the metallic component band at 1557 cm^{-1} were the sources of the G component, which includes the G(S) band, [19], [20].

3.1.2 FESEM and TEM Observations

The FESEM pictures of CNTs produced using various amounts of graphite and ferrocene (80:20, 70:30, 50:50, and 40:60) are shown in Fig. 4. The evaluation of the synthesized CNTs is based on their propensity for agglomeration and the formation of stacked bundles. For a 70:30 blend of graphite and ferrocene, the typical tube diameter is 45 nm.

The CNTs' cavity, as well as the top or bottom, is injected with encapsulated Fe catalyst nanoparticles (Fig. 4). According to a previous study, Fe nanoparticles were found to remain in a liquid state and be present inside the tube as dispersed heterogeneous metallic particles, [21]. Furthermore, microwave radiation that moved over the substrate surface and attached to the base of the CNTs decomposed the ferrocene into free Fe atoms[22]. The Fe sticks to the walls of the CNT due to the tube's strong capillary forces, [23]. Fig. 5 depicts an isolated CNT with graphitic caps and enclosed Fe nanoparticles aligned transversely to the CNT length. Additionally, it is shown that due to the buildup of Fe nanoparticles during CNT growth, the tube width of CNTs changes slightly over their length, [24].

3.1.3 X-ray Diffraction Analysis

The XRD analysis of CNT powder synthesized using graphite/ferrocene combination ratios of 80:20, 70:30, 50:50, and 40:60 is shown in Fig. 6. The prominent diffraction beak at 26.43o for all samples reveals the interlayer spacing of 0.34 A° of CNTs, according to JCPDS card number 00-008-0415. A decrease in CNT alignment is the cause of the (002) peak's higher intensity as compared to the other peaks. The other low-intensity minor peaks were associated with the hexagonal graphitic structure's reflections at 35.7°, 42.3°, 50.1°, 54.6°, and 77.4°, respectively.

Iron (Fe) and Fe carbide (Fe_3C) are both represented by the two peaks at (43.7° and 57°) and (44.6° and 62°), respectively, [25], [26], [27]. Fe_3C is employed as a progress indicator in the formation of nanotubes because it is thought to be an intermediary phase in the configuration of the graphite layers that make up CNTs, [28].

XRD line broadening can be used to determine the structural information of CNTs, [29], such as strain broadening, which is expressed by:

$$\gamma_d = \frac{\pi l}{d_c} \Delta d_c \quad (1)$$

where l is the index of reflection, is the interlayer spacing, and is the FWHM of the distribution of interlayer spacing. It is clear that the strain broadening brought on by the CNTs' curvature is greatly responsible for the reduction in the FWHM of (002) reflection. The Bragg law can be used to calculate the d-spacing of the (002) reflection, [30], [31]:

$$d_{hkl} = \frac{n\lambda}{2\sin\theta} \quad (2)$$

where n is the order of diffraction, λ is the X-ray wavelength,2θ stands for the scattering angle and d is the inter-planar spacing between the crystal planes.

The XRD data analysis of CNT synthesized using the microwave oven is summarized in Table 2. The strain (γ_d) of the grown CNT was calculated using Equation 1 and is listed in Table 2. CNT prepared using a 70:30 ratio of graphite/ferrocene showed the lowest strain value, [20], [29],

indicating a better quality crystal structure, the obtained results coincided with the Raman analysis.

3.2 CNT after Purification

3.2.1 FESEM and EDX Observation

The morphologies of "as-produced" CNTs (R-CNT) and functionalized CNTs (F-CNT) were comparatively analyzed using FESEM, as shown in Fig. 7. The surfaces and inside of the "as-produced" CNTs are shown to include amorphous carbon and iron particles (Fig. 7(a) and Figure 7(c)). The amorphous carbon and iron particles decreased significantly after the nitric acid treatment, as shown in Fig. 7(b) and Figure 7(d). The CNT shown in Fig. 8(b) and Figure 8(d) were analyzed using energy dispersive X-ray spectroscopy (EDX), and the results are displayed in Fig. 8(a) and Figure 8(c).

The EDX elemental analysis of the R-CNTs indicates the presence of C, O, and Fe, as outlined in Table 3. After oxidation and purification via HNO_3 acid treatment, the weight (%) of Fe in F-CNT decreased. In contrast, the quantity of O after treatment (F-CNTs) increased significantly compared to the "as-prepared" nanotubes. The CNTs tend to appear as bundles, as shown in the FESEM images, which is consistent with some previous studies, [32], [33]. Additionally, the introduction of a small number of functional groups, the partition of bundles of CNTs into some individual tubes, and generally smaller diameter bundles, as is evident in the FESEM images (Fig. 7(b) and Figure 7(d), can significantly increase the solubility of CNTs in ethanol (without adding surfactant or polymer conditions).

Fig. 9 shows a TEM image of CNTs after purification by HNO_3. It indicated that the majority of the iron particles embedded in the CNTs' tips had been eliminated. It appears that the metal catalyst was initially removed by nitric acid when the sealed tip was opened. The effectiveness of HNO_3 in removing metal particles is widely established, and it can eliminate amorphous carbon since it is a strong oxidant, [34].

3.2.2 Raman Spectroscopy Analysis

Fig. 10 displays the Raman spectra of the purified and "as-synthesized" CNTs. The full width at half maximum (FWHM) of the R-CNT and F-CNT, as well as the ratio of Raman band intensities, are shown in Table 4. It shows that the I_D/I_G ratio and FWHM of the G band decreased by 0.14 and 4.9, respectively, while the I_{2D}/I_D ratio increased by 0.55 for F-CNTs compared to as-synthesis CNTs. The ratios of the Raman peaks (I_D/I_G) generally decrease after purification because the removal of amorphous carbon improves the concentration of nanotubes. Furthermore, the I_D/I_G ratio is linearly correlated with the quantity of "disordered" carbon in the sample of graphitic materials. The decreased I_D/I_G and FWHM G as well as increased I_{2D}/I_D for F-CNTs indicate that oxidized amorphous carbon was transferred to the centrifuged suspension, where polyhedral carbon particles, Fe particles, highly crystallized graphite fragments, and a few large bundles of CNTs were deposited.

According to Cancado et al., the crystallite size L_a for nano graphitic by Raman spectroscopy was calculated from the following equation, [35]:

$$L_a(nm) = \frac{560}{{E_L}^4}\left(\frac{I_D}{I_G}\right)^{-1} \quad (3)$$

The excitation laser energy utilized in Raman spectroscopy is denoted as E_L and has a value of 1.96 eV.

The crystallite size has increased from 5.5 nm for R-CNT to 7.8 nm for F-CNT, as shown in Table 4.

3.2.3 FTIR Observation Analysis

Fig. 11 displays the FTIR spectra of the unfunctionalized and functionalized CNTs. The distinctive absorbance peak at 3553 cm^{-1} indicates the presence of -OH moieties or -OH in sorbed water and carboxyl groups.

The spectral bands observed in the 1550–1750 cm^{-1} range are indicative of C–C bonds present in aromatic rings and C–O groups present in different compounds such as ketone/quinone and carboxylic acid. On the other hand, the 950–1300 cm^{-1} range signifies C–O bonds present in various chemical environments, [36], [37]. The absorbance band at 1406 cm^{-1} comprises the OH in sorbed water and the C-O moiety, which are present as overlapping bands. The presence of OH sorbed during the production of carbon nanotubes is indicated by the weak bands observed at 2929 cm^{-1} and 1386 cm^{-1}, [38]. The functionalization of CNTs resulted in a decrease in the intensity of the -OH band at 3553 cm^{-1}. The absorbance band at 1406 cm^{-1} is comprised of the OH in sorbed water and the C-O moiety, which are present as overlapping bands. The presence of weak bands at 2929 cm^{-1} and 1386 cm^{-1} suggests the sorption of OH during the carbon

nanotube production process. The Fourier-transform infrared (FTIR) spectra of fluorinated carbon nanotubes (F-CNTs), as depicted in Fig. 11, suggest the presence of diverse hydroxyl groups that are bound to the sidewalls of the CNTs, [39], [40].

3.2.4 Electrical Properties

Fig. 12 illustrates the electrical performance of R-CNTs, and F-CNTs-based sensors observed between -5 V and +5 V. The current of F-CNTs" reached up to 35 mA as compared to 11 μA in R-CNTs, as the voltage was swept up to 5 V. Accordingly, the electrical transport properties of the F-CNTs are a thousand times greater than the R-CNTs. As a result of the functional groups attached to carbon nanotubes, there are more bands close to the Fermi level, which enhances electron transport between carbon atoms, [40].

4 Conclusion

CNT was successfully produced in a microwave oven using a combination of graphite and ferrocene as catalysts at room temperature in an ambient environment and the absence of feedstock or inert gases. The experimental results indicate that the structural quality is influenced by the graphite/ferrocene ratio. According to the I_D/I_G ratio values derived from Raman spectra, the CNTs with the best-improved crystallinity were generated using a graphite/ferrocene combination ratio of 70:30.

CNTs with an average diameter of 45 nm were produced, according to FESEM investigations. XRD analysis confirms that CNTs are stable in the presence of Fe and Fe_3C phases.

The electrical and morphological properties of the CNT were improved by removing the metal particles using nitric acid (HNO_3, 2.6 M) and the remaining amorphous carbon and graphite particles using the centrifugation technique. The amount of residual catalyst in purified CNT was removed, as displayed by TEM. Fe concentration in F-CNT was reduced, and the quantity of O content sharply increased after oxidation and purification. The FTIR and measurements exhibit the presence of a hydroxyl group linked to the surfaces of the CNT. The functionalization of carbon nanotubes resulted in an increase in electrical current from 11 μA for F-CNT to 35 mA for R-CNT.

Acknowledgment:
This work has been supported by Isra University and Al-Zaytoonah University of Jordan, Amman, Jordan.

References:

[1] J. Prasek, J. Drbohlavova, J. Chomoucka, J. Hubalek, O. Jasek, V. Adam, *et al.*, "Methods for carbon nanotubes synthesis—review," *Journal of Materials Chemistry,* vol. 21, pp. 15872-15884, 2011.

[2] S. Sharifi, N. N. Mahmoud, E. Voke, M. P. Landry, and M. Mahmoudi, "Importance of Standardizing Analytical Characterization Methodology for Improved Reliability of the Nanomedicine Literature," *Nano-Micro Letters,* vol. 14, pp. 1-15, 2022.

[3] D. Jones, T. Lelyveld, S. Mavrofidis, S. Kingman, and N. Miles, "Microwave heating applications in environmental engineering—a review," *Resources, conservation and recycling,* vol. 34, pp. 75-90, 2002.

[4] Z. Liu, J. Wang, V. Kushvaha, S. Poyraz, H. Tippur, S. Park, *et al.*, "Poptube approach for ultrafast carbon nanotube growth," *Chemical Communications,* vol. 47, pp. 9912-9914, 2011.

[5] M. Daenen, R. De Fouw, B. Hamers, P. Janssen, K. Schouteden, and M. Veld, "The wondrous world of carbon nanotubes," *Eindhoven University of Technology,* vol. 27, 2003.

[6] S. C. Tjong, *Carbon nanotube reinforced composites: metal and ceramic matrices*: John Wiley & Sons, 2009.

[7] F. Li, H. Cheng, Y. Xing, P. Tan, and G. Su, "Purification of single-walled carbon nanotubes synthesized by the catalytic decomposition of hydrocarbons," *Carbon,* vol. 38, pp. 2041-2045, 2000.

[8] A. Yu, E. Bekyarova, M. E. Itkis, D. Fakhrutdinov, R. Webster, and R. C. Haddon, "Application of centrifugation to the large-scale purification of electric arc-produced single-walled carbon nanotubes," *Journal of the American Chemical Society,* vol. 128, pp. 9902-9908, 2006.

[9] Y. Liu, L. Gao, J. Sun, S. Zheng, L. Jiang, Y. Wang, *et al.*, "A multi-step strategy for cutting and purification of single-walled

carbon nanotubes," *Carbon,* vol. 45, pp. 1972-1978, 2007.

[10] A. M. Al-Diabat, N. A. Algadri, N. M. Ahmed, A. Abuelsamen, and S. A. Bidier, "A high-sensitivity hydrogen gas sensor based on carbon nanotubes fabricated on SiO2 substrate," *Nanocomposites,* vol. 7, pp. 172-183, 2021.

[11] V. Shanov, Y.-H. Yun, and M. J. Schulz, "Synthesis and characterization of carbon nanotube materials," *Journal of the University of Chemical Technology and Metallurgy,* vol. 41, pp. 377-390, 2006.

[12] L. Dai, *Carbon nanotechnology: recent developments in chemistry, physics, materials science and device applications*: Elsevier, 2006.

[13] M. K. Kumar and S. Ramaprabhu, "Palladium dispersed multiwalled carbon nanotube based hydrogen sensor for fuel cell applications," *International Journal of Hydrogen Energy,* vol. 32, pp. 2518-2526, 2007.

[14] S. Santangelo, G. Messina, G. Faggio, S. Abdul Rahim, and C. Milone, "Effect of sulphuric–nitric acid mixture composition on surface chemistry and structural evolution of liquid- phase oxidised carbon nanotubes," *Journal of Raman Spectroscopy,* vol. 43, pp. 1432-1442, 2012.

[15] K. A. Wepasnick, B. A. Smith, K. E. Schrote, H. K. Wilson, S. R. Diegelmann, and D. H. Fairbrother, "Surface and structural characterization of multi-walled carbon nanotubes following different oxidative treatments," *Carbon,* vol. 49, pp. 24-36, 2011.

[16] H. Hu, B. Zhao, M. E. Itkis, and R. C. Haddon, "Nitric acid purification of single-walled carbon nanotubes," *The Journal of Physical Chemistry B,* vol. 107, pp. 13838-13842, 2003.

[17] S. Brown, A. Jorio, M. Dresselhaus, and G. Dresselhaus, "Observations of the D-band feature in the Raman spectra of carbon nanotubes," *Physical Review B,* vol. 64, p. 073403, 2001.

[18] K. Żelechowska, B. Trawiński, S. Dramińska, D. Majdecka, R. Bilewicz, and B. Kusz, "Oxygen biosensor based on carbon nanotubes directly grown on graphitic substrate," *Sensors and Actuators B: Chemical,* vol. 240, pp. 1308-1313, 2017.

[19] S. Brown, A. Jorio, a. P. Corio, M. Dresselhaus, G. Dresselhaus, R. Saito, *et al.*, "Origin of the Breit-Wigner-Fano lineshape of the tangential G-band feature of metallic carbon nanotubes," *Physical Review B,* vol. 63, p. 155414, 2001.

[20] D. K. Singh, P. Iyer, and P. Giri, "Diameter dependence of interwall separation and strain in multiwalled carbon nanotubes probed by X-ray diffraction and Raman scattering studies," *Diamond and Related Materials,* vol. 19, pp. 1281-1288, 2010.

[21] X. Chen, R. Wang, J. Xu, and D. Yu, "TEM investigation on the growth mechanism of carbon nanotubes synthesized by hot-filament chemical vapor deposition," *Micron,* vol. 35, pp. 455-460, 2004.

[22] P. B. Amama, C. L. Pint, L. McJilton, S. M. Kim, E. A. Stach, P. T. Murray, *et al.*, "Role of water in super growth of single-walled carbon nanotube carpets," *Nano Letters,* vol. 9, pp. 44-49, 2008.

[23] P. M. Ajayan, "Capillarity-induced filling of carbon nanotubes," *Nature,* vol. 361, pp. 333-334, 1993.

[24] R. Bajpai and H. D. Wagner, "Fast growth of carbon nanotubes using a microwave oven," *Carbon,* vol. 82, pp. 327-336, 2015.

[25] Y. Chen, M. Conway, J. F. Gerald, J. Williams, and L. Chadderton, "The nucleation and growth of carbon nanotubes in a mechano-thermal process," *Carbon,* vol. 42, pp. 1543-1548, 2004.

[26] A. Cao, C. Xu, J. Liang, D. Wu, and B. Wei, "X-ray diffraction characterization on the alignment degree of carbon nanotubes," *Chemical Physics Letters,* vol. 344, pp. 13-17, 2001.

[27] W. Li, C. Liang, W. Zhou, J. Qiu, Z. Zhou, G. Sun, *et al.*, "Preparation and characterization of multiwalled carbon nanotube-supported platinum for cathode catalysts of direct methanol fuel cells," *The Journal of Physical Chemistry B,* vol. 107, pp. 6292-6299, 2003.

[28] A. K. Schaper, H. Hou, A. Greiner, and F. Phillipp, "The role of iron carbide in multiwalled carbon nanotube growth," *Journal of Catalysis,* vol. 222, pp. 250-254, 2004.

[29] D. Reznik, C. Olk, D. Neumann, and J. Copley, "X-ray powder diffraction from carbon nanotubes and nanoparticles," *Physical review B,* vol. 52, p. 116, 1995.

[30] J. A. Davis and J. O. Leckie, "Surface ionization and complexation at the oxide/water interface II. Surface properties of amorphous iron oxyhydroxide and adsorption of metal ions," *Journal of Colloid and Interface Science,* vol. 67, pp. 90-107, 1978.

[31] N. A. Algadri, A. M. Al-Diabat, and N. M. Ahmed, "High sensitive UV photodetector based on ZnS/PS thin film prepared via spray pyrolysis method," *Energy Sources, Part A: Recovery, Utilization, and Environmental Effects,* vol. 44, pp. 5303-5313, 2022.

[32] P. Wick, P. Manser, L. K. Limbach, U. Dettlaff-Weglikowska, F. Krumeich, S. Roth, *et al.*, "The degree and kind of agglomeration affect carbon nanotube cytotoxicity," *Toxicology letters,* vol. 168, pp. 121-131, 2007.

[33] A. Vignes, O. Dufaud, L. Perrin, D. Thomas, J. Bouillard, A. Janes, *et al.*, "Thermal ignition and self-heating of carbon nanotubes: From thermokinetic study to process safety," *Chemical Engineering Science,* vol. 64, pp. 4210-4221, 2009.

[34] C.-M. Chen, M. Chen, F.-C. Leu, S.-Y. Hsu, S.-C. Wang, S.-C. Shi, *et al.*, "Purification of multi-walled carbon nanotubes by microwave digestion method," *Diamond and related materials,* vol. 13, pp. 1182-1186, 2004.

[35] L. Cançado, K. Takai, T. Enoki, M. Endo, Y. Kim, H. Mizusaki, *et al.*, "General equation for the determination of the crystallite size L a of nanographite by Raman spectroscopy," *Applied Physics Letters,* vol. 88, p. 163106, 2006.

[36] L. Stobinski, B. Lesiak, L. Kövér, J. Tóth, S. Biniak, G. Trykowski, *et al.*, "Multiwall carbon nanotubes purification and oxidation by nitric acid studied by the FTIR and electron spectroscopy methods," *Journal of Alloys and Compounds,* vol. 501, pp. 77-84, 2010.

[37] M. N. Tchoul, W. T. Ford, G. Lolli, D. E. Resasco, and S. Arepalli, "Effect of mild nitric acid oxidation on dispersability, size, and structure of single-walled carbon nanotubes," *Chemistry of Materials,* vol. 19, pp. 5765-5772, 2007.

[38] S.-Z. Kang, D.-e. Yin, X. Li, and J. Mu, "A facile preparation of multiwalled carbon nanotubes modified with hydroxyl groups and their high dispersibility in ethanol," *Colloids and Surfaces A: Physicochemical and Engineering Aspects,* vol. 384, pp. 363-367, 2011.

[39] J. Zhang, H. Zou, Q. Qing, Y. Yang, Q. Li, Z. Liu, *et al.*, "Effect of chemical oxidation on the structure of single-walled carbon nanotubes," *The Journal of Physical Chemistry B,* vol. 107, pp. 3712-3718, 2003.

[40] S. Dhall, N. Jaggi, and R. Nathawat, "Functionalized multiwalled carbon nanotubes based hydrogen gas sensor," *Sensors and Actuators A: Physical,* vol. 201, pp. 321-327, 2013.

Appendix

Fig. 1: CNT treatment steps

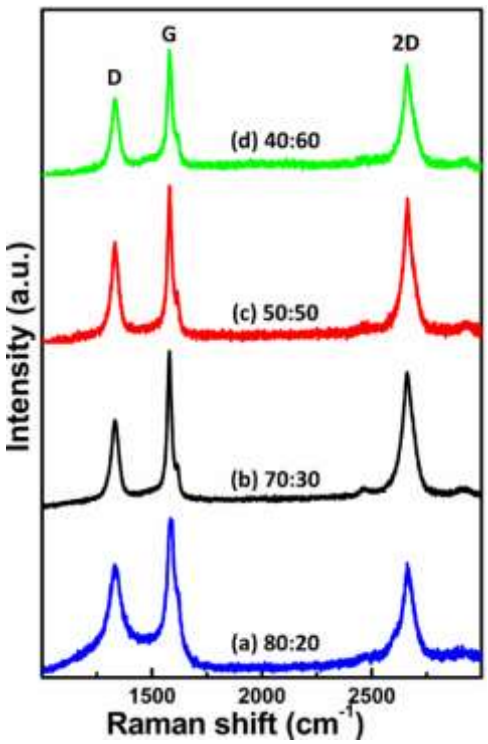

Fig. 2: Raman spectra for graphite/ferrocene ratios of (a) 80:20 (b) 70:30 (c) 50:50 (d) 40:60 for CNTs produced by microwave oven in the range of 1000-3000 cm^{-1}

Ahmad M. Al-Diabat, Natheer A. Algadri,
Naser M. Ahmad, Adnan H. Alrajhi,
Abdulsalam Abuelsamen, Amal Mohamed Ahmed Ali,
Salma Abdulrhman Al-Wasli

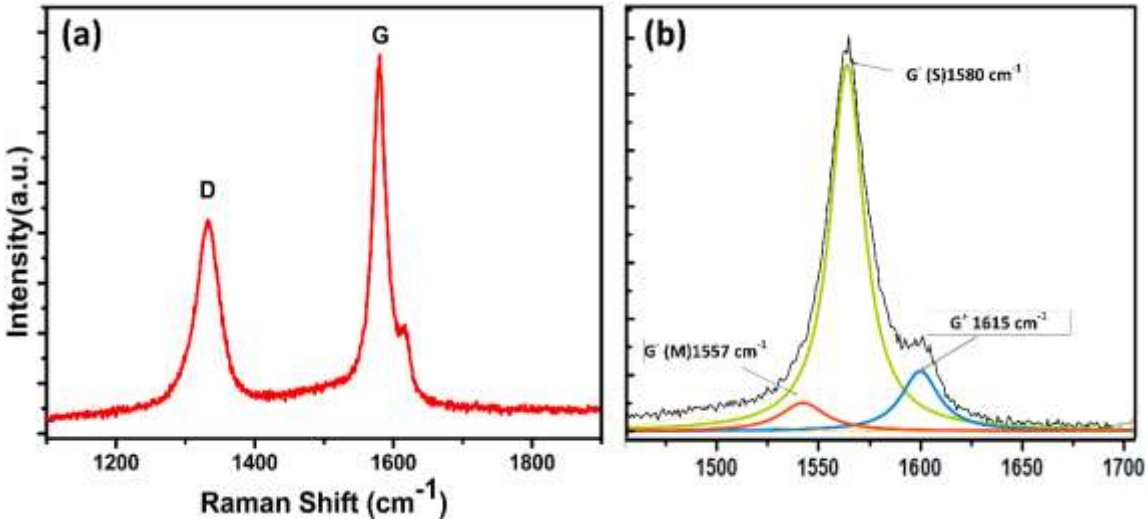

Fig. 3: (a) Raman spectra for CNTs produced by microwave oven at a ratio of 70:30, obtained in the range between 1100 and 1900 cm^{-1},(b) CNTs' Raman spectra show the optical phonon mode G-band at a wavelength of about 1580 cm-1. Three components are displayed through lorentzian fitting (color lines)

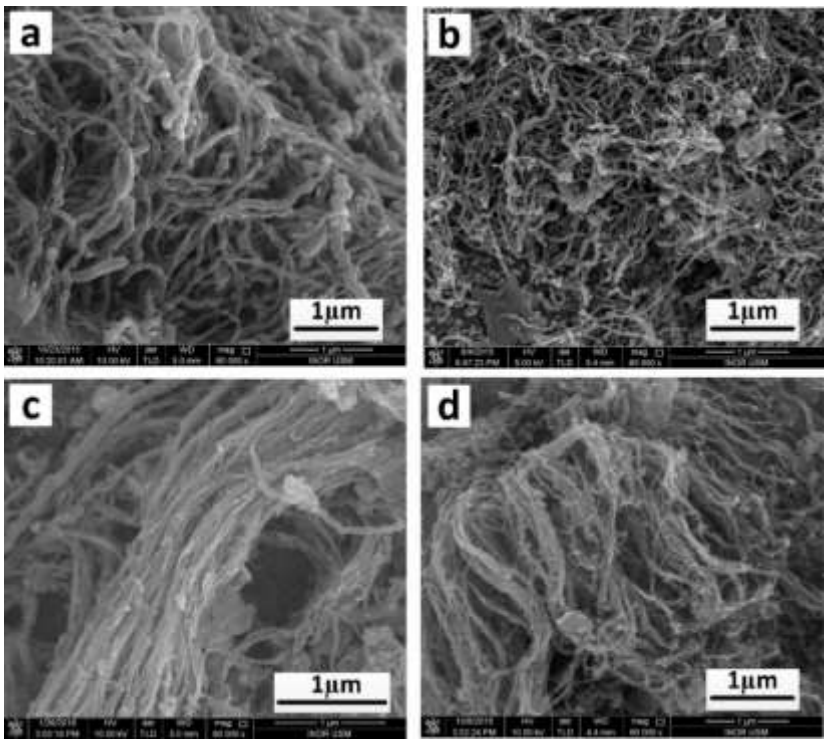

Fig. 4: Shows FESEM images of CNTs produced by microwave irradiating mixtures of graphite and ferrocene at ratios of (a) 80:20, (b) 70:30, (c) 50:50, and (d) 40:60 for 5 seconds

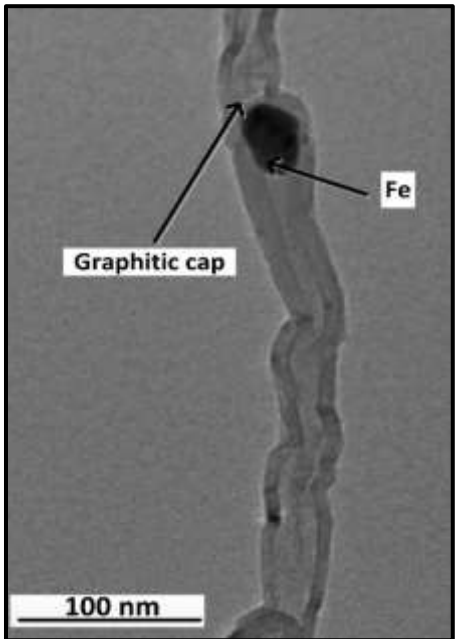

Fig. 5: TEM picture of a CNT produced by a microwave oven using a 70:30 powder mixture of graphite and ferrocene

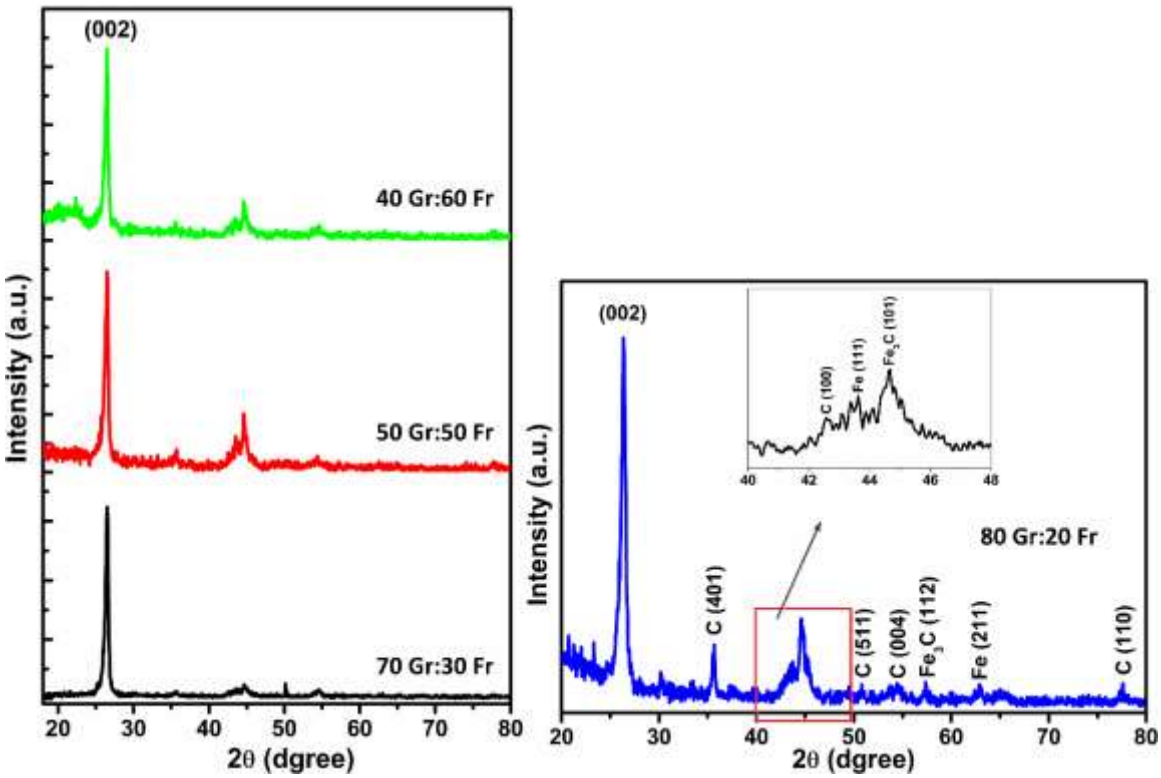

Fig. 6: X-ray diffraction of CNTs powder produced from a mixture of graphite and ferrocene with ratios of 80:20, 70:30, 50:50, and 40:60

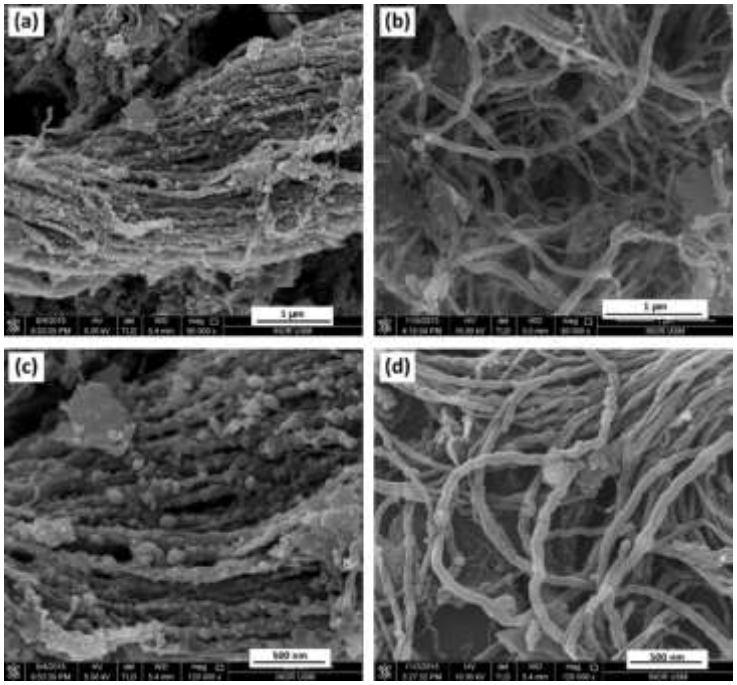

Fig. 7: FESEM images of untreated CNT (a) and (c), and HNO_3-treated CNT (b) and (d).

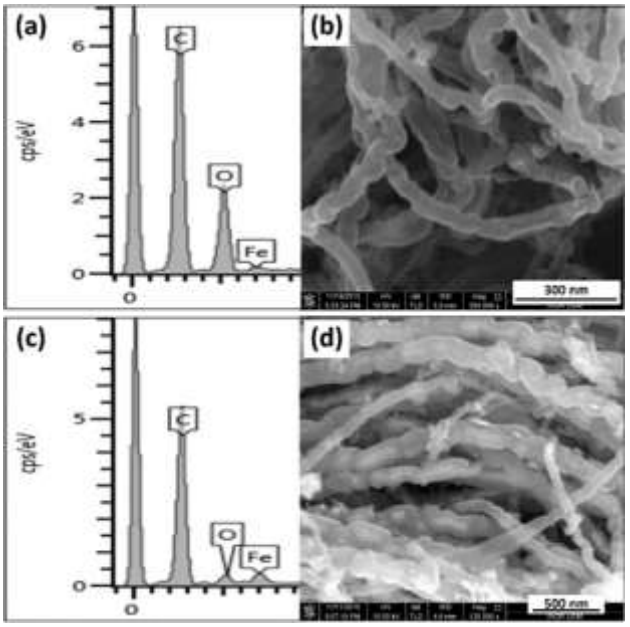

Fig. 8: Acid treated CNT and as-prepared CNT were analyzed using EDX in (a) and (c) and FESEM in (b) and (d), respectively

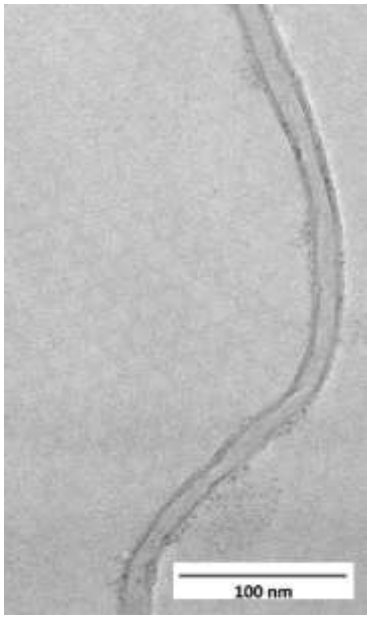

Fig. 9: TEM image of CNTs after purification by HNO_3

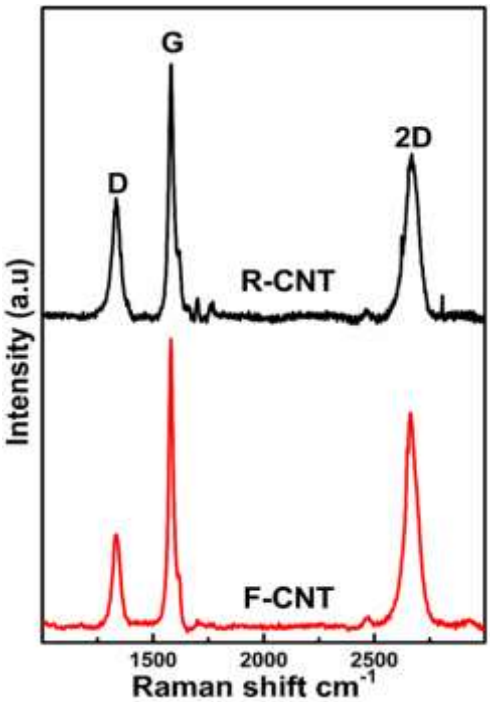

Fig. 10: The Raman spectra of "as-prepared" (R-CNT) and functionalized carbon nanotube (F-CNT)

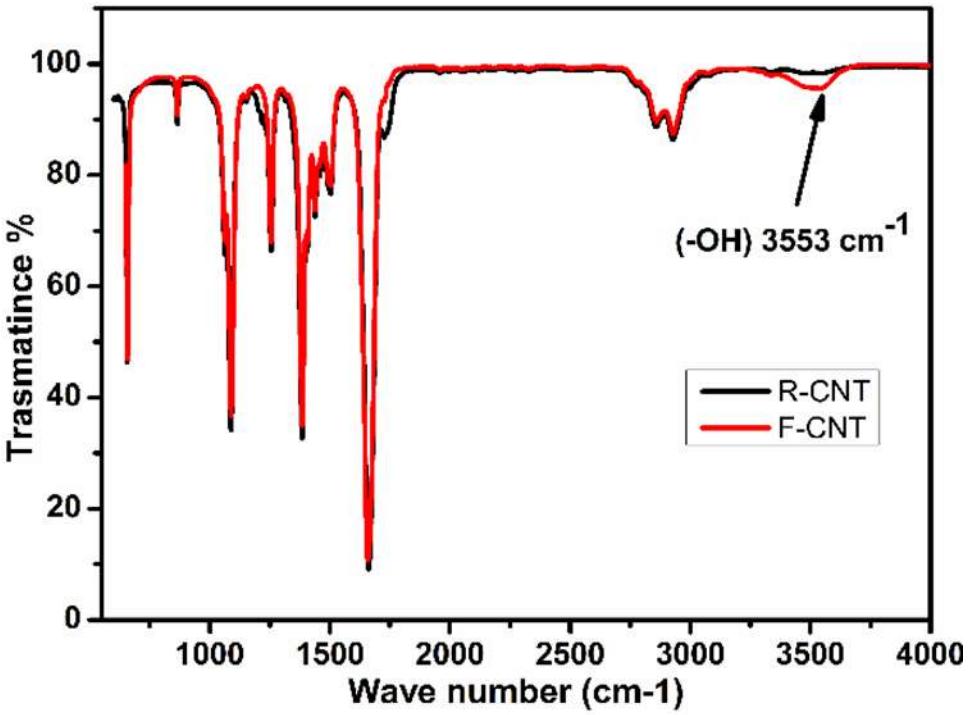

Fig. 11: The FTIR spectra of "as-produced" (R-CNT) and acid treated carbon nanotube (F-CNT)

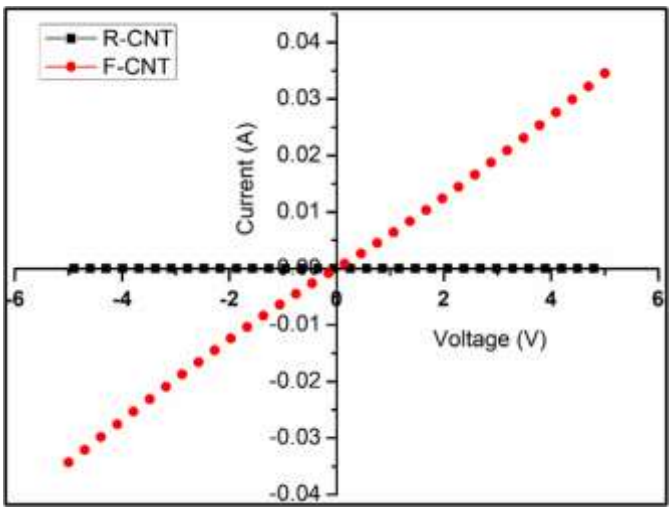

Fig. 12: Comparison of I-V characteristics of R-CNTs and F-CNTs at 5V

Table 1. Comparison of Raman spectrum intensities for CNTs produced using deferent ratio of graphite/ferrocene

Gr: Fr	80:20	70:30	50:50	40:60
I_D/I_G	0.64	0.47	0.77	0.70
I_{2D}/I_D	1.28	1.45	1.25	1.29
FWHM G	40.65	34.4	41.90	35.82

Table 2. X-ray diffraction analysis for the produced CNT using graphite/ferrocene with different ratio

Sample Ratio Gr:Fr	2θ Degree	FWHM (002) (º)	d(002) (Å)	γ_d
80:20	26.47	0.64	3.367	1.194
70:30	26.41	0.51	3.375	0.949
50:50	26.53	0.59	3.360	1.103
40:60	26.46	0.56	3.368	1.045

Table 3. EDX analysis of as-produced CNT and acid treated CNT

Element	Weight%	
	R-CNT	F-CNT
C	71.2	63.71
O	5.18	32.03
Fe	23.61	4.25

Table 4. Comparison of Raman spectrum intensities and FWHM of G-band for R-CNTs and F-CNT

properties	R-CNT	F-CNT
I_D/I_G	0.47	0.33
I_{2D}/I_D	1.45	2
FWHM G	34.4	29.5
L_a (nm)	5.5	7.8

Contribution of Individual Authors to the Creation of a Scientific Article (Ghostwriting Policy)

The authors equally contributed to the present research, at all stages from the formulation of the problem to the final findings and solution.

Sources of Funding for Research Presented in a Scientific Article or Scientific Article Itself

No funding was received for conducting this study.

Conflict of Interest

The authors have no conflicts of interest to declare.

Creative Commons Attribution License 4.0 (Attribution 4.0 International, CC BY 4.0)

This article is published under the terms of the Creative Commons Attribution License 4.0
https://creativecommons.org/licenses/by/4.0/deed.en_US